Available online at www.sciencedirect.com
ScienceDirect
Journal of the European Ceramic Society 29 (2009) 3079–3090
www.elsevier.com/locate/jeurceramsoc

Polymer-derived mullite–SiC-based nanocomposites

Ralf Riedel *, Liviu Toma, Claudia Fasel, Gerhard Miehe

Fachbereich Material- und Geowissenschaften, Fachgebiet Disperse Feststoffe, Technische Universität Darmstadt, 64287 Darmstadt, Germany

Received 19 December 2008; received in revised form 30 April 2009; accepted 13 May 2009
Available online 18 June 2009

Abstract

Ceramic mullite–SiC nanocomposites were successfully produced at temperatures below 1500 °C by the polymer pyrolysis technique. An alumina-filled poly(methylsilsesquioxane) compound was prepared by mechanically mixing and cross-linking via a catalyst prior to pyrolysis. Heat treatment of warm pressed alumina/polymer bulk samples under the exclusion of oxygen (inert argon atmosphere) up to 1500 °C initiated crystallization of mullite even at pyrolysis temperatures as low as 1300 °C. The influence of the filler and of the pyrolysis temperature on the crystallization behavior of the materials has been investigated. Based on thermal analysis in combination with elemental analysis and X-ray powder diffraction studies four polymer mixtures differing in type and content of nano-alumina powders were examined. Nano-sized γ-Al_2O_3 powders functionalized at the surface by octylsilane groups proved to be more reactive towards the preceramic polymer leading to the formation of a larger weight fraction of mullite crystals at lower processing temperatures (1300 °C) as compared to native nano-γ-Al_2O_3 filler. Moreover, the functionalized nano-alumina particles offer an enhanced homogeneity of the distribution of alumina nano-particles in the starting polysiloxane system. In consequence, the received ceramic samples exhibited a nano-microstructure consisting of crystals of mullite with an average dimension in the range of 60–160 nm and silicon carbide crystals in the range of 1–8 nm.

Keywords: Polymer-derived ceramics; Mullite; Silicon carbide (SiC); Ceramic nanocomposites

1. Introduction

In recent years ceramic nanocomposites have attracted great scientific and technological attention due to an improvement in mechanical properties such as hardness, strength and wear resistance, along with the possibility of superplasticity, as compared with the monolithic matrix material.[1] Ceramic nanocomposites may be useful as structural and functional materials for a variety of applications in different fields of technology. To retain their superior properties up to high temperatures is a major technological challenge. In the last years mullite with the composition $2SiO_2 \times 3Al_2O_3$ in particular and the Al_2O_3–SiO_2 system in general have become challenging materials in the fields of structural and optoelectronic applications.[2,3] The special features of mullite-based ceramics are related to its high refractoriness and its good thermomechanical properties, low thermal expansion and conductivity, as well as to its excellent oxidation and heat resistance. However mullite has a low fracture toughness ($K_{IC} = 2.5\ MPa\ m^{1/2}$) and low bending strength ($\sigma_B = 350\ MPa$). The incorporation of a nano-sized second phase particles such as SiC into the mullite matrix can lead to an improvement of its mechanical properties.[4,5] It is also known that mullite–SiC composites show damage self-healing characteristics as reported by Ando et al.[6] and Takahashi et al.[7] The observed enhanced properties strongly fluctuate with the dimension of the sizes of the phases present in the ceramic nanocomposite.[4] To control the properties of nanocomposites requires well established and reliable routes of processing methodologies. Generally, bulk nanocomposites can be fabricated by conventional powder processing, sol–gel and polymer pyrolysis techniques. In particular, mullite–SiC nanocomposites were reported to be formed by the first two methods[8,9] while little is known regarding the polymer pyrolysis method. Low processing temperatures and the possibility of using polymer forming techniques to get complex shapes are the main advantages of the polymer-to-ceramic transformation process.[10–14]

Here we report on the preparation of homogeneous mullite–SiC nanocomposites formed at unusual low temperatures from a selected mixture of polysiloxane preceramic polymer and alumina nanopowders. The aim of this work is also to study

* Corresponding author. Tel.: +49 6151 16 6347; fax: +49 6151 16 6346.
E-mail address: riedel@materials.tu-darmstadt.de (R. Riedel).

0955-2219/$ – see front matter © 2009 Elsevier Ltd. All rights reserved.
doi:10.1016/j.jeurceramsoc.2009.05.016

the influence of the type of nano-Al_2O_3-precursor, namely its polymorphism, particle size and surface functionality on the crystallization behavior of the compacted preceramic polymer compound with respect to the development of mullite–SiC nanocomposite ceramics. The thermal decomposition of the preceramic polymer/alumina mixture with temperature has been studied by thermogravimetric analysis (TGA), differential thermal analysis (DTA), and in situ evolved gas analysis using mass spectrometry (MS). The structural evolution was followed up by X-ray diffraction (XRD) in combination with Rietveld refinement as well as with micro-Raman spectroscopy. The microstructure of the pyrolyzed ceramics has been investigated by electron microscopy (SEM and TEM).

2. Experimental procedure

Commercially available poly(methylsilsesquioxane) (Wacker-Belsil^{TM} PMS MK®) was used as the starting preceramic polymer. The PMS MK polymer is a solid silicone resin, solvent free, and can be described by the following basic composition: $(CH_3–SiO_{3/2})_x$. The polymer possesses approximately 2 mol% hydroxyl- and ethoxyl-groups as functional units and has a softening range between 45 and 60 °C. It exhibits a good solubility in organic solvents, namely aromatic solvents and ketones. With the evolution of water and ethanol by polycondensation reactions, the formation of a three dimensionally cross-linked network with Si–O–Si alternating units as the backbone takes place. In order to achieve an acceptable process regime, the addition of a suitable catalyst agent in sufficient amount and a distinct thermal treatment are necessary. Zirconium acetylacetonate ($C_{20}H_{28}O_8Zr$, referred as catalyst) in 1 wt% related to the polymer mass was used as cross-linking agent. The polymer was dissolved in acetone along with 1 wt% catalyst and the solution was stirred by a magnetic stirrer for 30 min, followed by a sonication step for further 30 min to achieve a homogeneous distribution of the catalyst in the polymer. Subsequently the solution was dried under vacuum at moderate temperature (40–50 °C). The crude preceramic polymer powder was dried in air for about 24 h, ball milled at 180 rpm for one h and finally sieved to a particle size <100 μm.

For the further experiments two different γ-alumina nanoparticles were used as fillers: the Aeroxide® Alu C (Evonic Industries, Germany), a very fine metal oxide (γ-alumina) with a high specific surface area and an average particle size of 13 nm, and Aeroxide® Alu C805 (Evonic Industries, Germany), a γ-alumina treated with octylsilane (highly dispersed hydrophobic metal oxide with 3–4.5% carbon content and 13 nm particle size, respectively). Four samples were prepared: AMK1 (25 vol.% Aeroxide® Alu C+ 75 vol.% MK polymer), AMK2 (37 vol.% Aeroxide® Alu C+ 67 vol.% MK polymer), AFMK1 (30 vol.% Aeroxide® Alu C805+ 70 vol.% MK polymer) and AFMK2 (37 vol.% Aeroxide® Alu C805+ 67 vol.% MK polymer). The catalytically treated polymer is mixed with the respective alumina filler by ball milling at 180 rpm for 1 h and the mixture is finally sieved to a particle size <100 μm. Shaping of the powder mixture and cross-linking of the poly(methylsilsesquioxane) to an infusible polymer mass with a three dimensional network of polymer chains is achieved simultaneously by warm pressing under pressure and high temperature in a metallic die. Green bodies (Fig. 1) were prepared in a rectangular mold (40 mm × 30 mm) by warm pressing at 25 MPa and 180 °C. Pressure was applied with a hydraulic press (warm press type 123, H. Collin) with a maximum load of 50 kN. Subsequently the preceramic bulk samples were pyrolyzed under flowing argon atmosphere in a tube furnace (HTSS 100-500, Gero Hochtemperaturöfen GmbH), equipped with a sealed alumina tube and inert argon gas flow system up to the pyrolysis temperature of 1100, 1200 or 1300 °C (Fig. 1). The following heating program was used: heating rate of 50 °C/h up to 200 °C, 25 °C/h up to 900 °C, and 50 °C/h to the final temperature. The holding time at the final temperature was 3 h followed by a cooling rate of 300 °C/h down to room temperature.

Further annealing treatments were performed on bulks in open alumina crucible to analyze the crystallization behavior. The selected samples (bulk materials pyrolyzed at 1300 °C) were heated up to 1400 °C or 1500 °C in a HTM Reetz LORA 32/1000 furnace with 10 °C/min in argon atmosphere and held at the maximum temperature for 3 h.

The pyrolytic transformation from the polymer to the ceramic was studied for the green body material by simultaneous thermal analysis (DTA/TG) using a Netzsch STA 449C *Jupiter*® equipment operating in argon flow (25 ml/min) with a heating rate of 5 °C/min up to the maximum temperature of about 1400 °C. Analyses of the evolved gases were obtained in situ using a coupled quadrupole mass spectrometer (QMS 403C Aëolos).

The carbon content of the powdered ceramic samples was determined by combustion analysis with a carbon analyzer (Leco, Type C-200). The oxygen content of the powdered ceramic samples was determined by hotgas extraction with N/O analyzer (Leco, Type TC-436). Aluminium and silicon content was estimated by difference to 100% presuming that no alumina is lost during the pyrolysis and taking into account the weight loss during pyrolysis.

X-ray powder diffraction analyses (model STADI P in transmission/Debye–Scherrer geometry with linear PSD, STOE, Darmstadt, Germany) were performed with powdered samples using a curved Ge (1 1 1) monochromator and Cu Kα radiation. X-ray patterns were taken by measuring 2θ from 10° to 90° with a step size of 0.030° and a step time of 5 s. The quantitative determination of mullite in the ceramic samples was achieved from X-ray diffraction data by using Rietveld refinement. It was performed with Fullprof, available in the software package Winplotr.[15] The refinement involved the following parameters: a scale factor, zero displacement correction, background, unit cell parameters, peak profile parameters using a pseudo-Voight function and overall temperature factor. Instrumental contributions to peak broadening were determined using Si as a standard reference material. The structural parameters and atomic positions for mullite, silicon carbide, cristobalite and gamma phase of alumina were taken from the literature.[16–19]

The skeletal density of the compacts was measured by the Archimedes method with distilled water as immersion liquid (samples were boiled in water before the measurements). The bulk density was calculated by the ratio mass over volume. Open

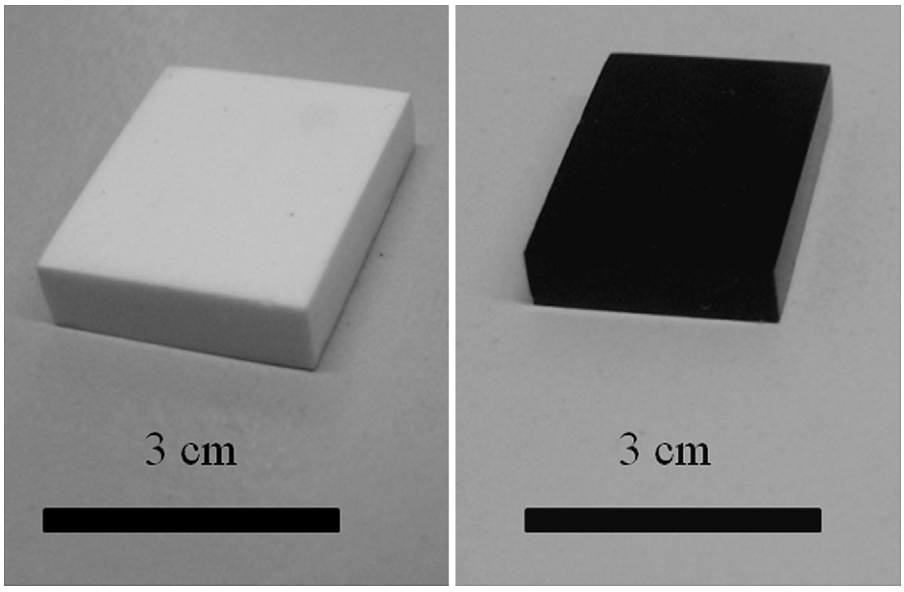

Fig. 1. Green body and pyrolyzed AFMK2 samples.

porosity was determined by the ratio bulk/skeletal density. The relative density was calculated using the theoretical densities of alumina (3.96 g cm^{-3}), silicon carbide (3.20 g cm^{-3}) and mullite (3.19 g cm^{-3}).

Scanning electron microscopy measurements were performed on a JEOL 6300F SEM microscope at 5 kV. Specimens were prepared by first embedding the sample followed by a polishing phase and at the end etching for 15 min in a Polaron PT7100 RF plasma barrel etcher. The samples were dried in vacuum at room temperature and measured after being sputtered with a thin gold layer.

Transmission electron microscopy (TEM) imaging and electron diffraction pattern (EDP) analysis were performed on TEM-foils obtained from the pyrolyzed and annealed SiOC bulk samples. Sample preparation followed the standard ceramographic technique of cutting, ultrasonic drilling, dimpling and Ar-ion thinning to perforation followed by light carbon coating to minimize charging under the incident electron beam. The instrument used was a Philips CM20STEM (FEI, Eindhoven, The Netherlands) operating at 200 keV.

Micro-Raman spectra were recorded on a Horiba HR800 micro-Raman spectrometer using an excitation laser wavelength of 514 nm. Spectra were obtained with a 100× objective and an accumulation of 3 s was used.

3. Results and discussion

The controlled pyrolysis of preceramic polysiloxane filled with alumina nano-particles results in the formation of mullite/SiC-based nanocomposites. One major advantage of applying the polymer pyrolysis technique is that homogeneous polymeric green compacts can be prepared, which are subsequently transformed into mullite-based nanocomposites at relatively low temperatures. In addition, the proposed processing method combines the advantages of polymer processing and the reactivity of nano-particles. In this way the γ-alumina and functionalized γ-alumina nano-particles are mixed with a commercially available preceramic polymer using a simple dispersion method. The precursor powders are stable and, as they contain a cross-linkable and meltable polymer, can be processed using conventional shaping technologies (e.g., cold or warm pressing, extrusion, spinning, etc.).

In our study, a relatively high volume fraction of alumina powders was added to the preceramic polymer (up to 37 vol.%) to investigate if, in the presence of the right amount of nano-alumina particles, the entire amount of silica intrinsically present in the SiOC matrix obtained from pyrolysis of the preceramic volume fraction can be converted to mullite under the selected pyrolysis conditions. The choice of γ-Al_2O_3 instead of α-Al_2O_3 was first of all related to the size of the commercially available alumina powders which are 13 nm for the γ-phase in comparison with 300 nm for the α-phase.[20–22] Furthermore, it is known that high density mullite ceramics can be produced at relatively low temperature by the pyrolysis of polysiloxane filled with γ-alumina powders in air. Our interest in the functionalized γ-alumina powder was to study the effect of the hydrophobic surface of the particles with respect to their reactivity towards the silica matrix. The choice of the pyrolysis atmosphere, namely argon in our case, is essential for the production of oxide/nonoxide nanocomposites from preceramic polymers. A review of the existing literature showed that there are a few reports related to mullite formation from sol–gel or from polymer pyrolysis by the thermal decomposition of polysiloxanes in the presence of alumina powders in air.[20–24] It is also known that pyrolysis of polysiloxanes under argon atmosphere provides the formation of silicon carbide beyond 1300 °C.[25]

The polymer-to-ceramic transformation of our prepared composite samples was investigated by thermogravimetric analysis (TGA) and differential thermal analysis (DTA). As a representative example, the results obtained with the AMK2 green body bulk sample are shown in Fig. 2. Accordingly, the material exhibits a total weight loss of 7.35% occurring in four

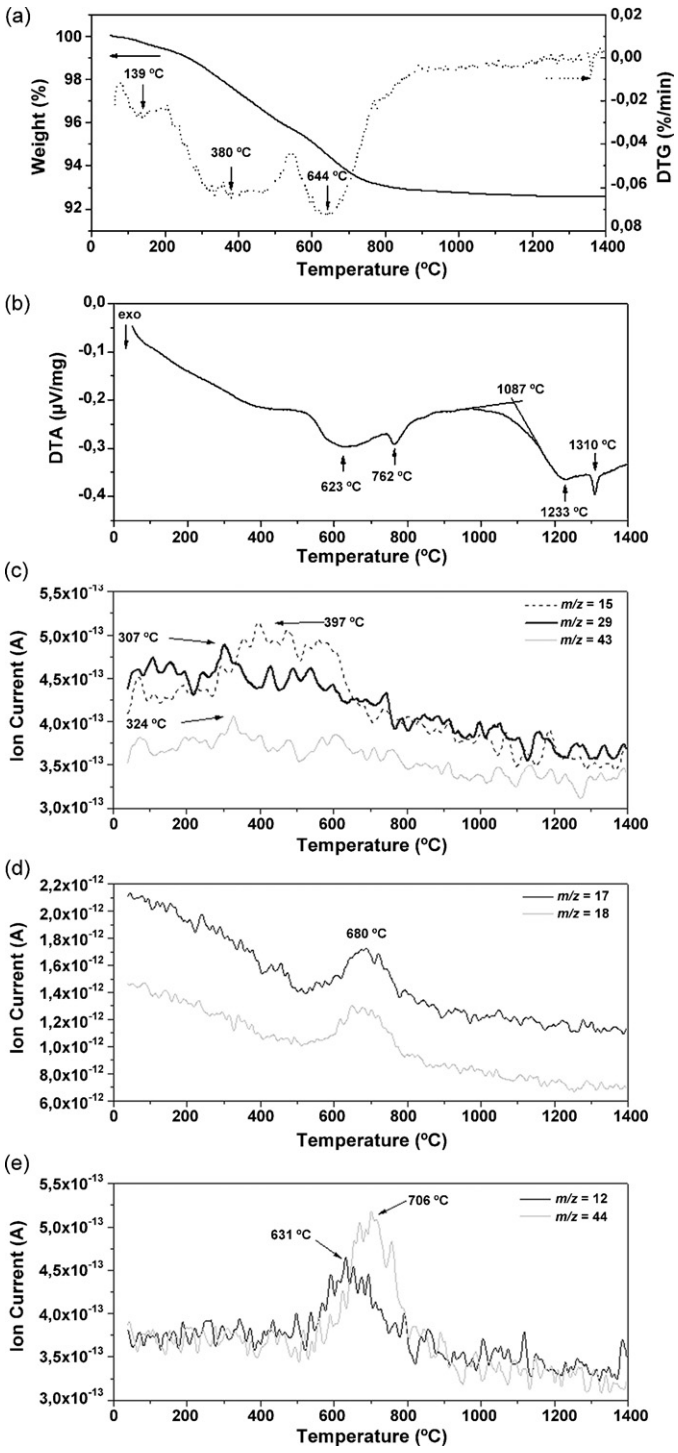

Fig. 2. Thermal analysis of the AMK2 sample; (a) TG with its first derivative plot (DTG); (b) DTA curve and in situ mass spectroscopy with (c) methane evolution and acetone decomposition $m/z = 15$, $m/z = 29$ and $m/z = 43$; (d) water evaporation $m/z = 17$, $m/z = 18$; (e) CO_2 release $m/z = 12$ and $m/z = 44$.

steps: 0.51% in the region 70–190 °C, 3.72% between 190 and 550 °C and 2.85% between 550 and 900 °C and finally a further weight loss in the amount of 0.27% is detected up to the final temperature of 1400 °C. The first three regions of weight loss can be attributed to different single processes as visualized by the plot of the first derivative (DTG) of the thermogravimetric curve in Fig. 2(a). Investigations of the pure polymer have shown that the first and the second weight loss stages are caused by polycondensation reactions which occur in the silicone resin during cross-linking releasing water, ethanol and methanol as byproducts.[25] Moreover, the mass loss can be correlated with an additional release of low mass organic fraction which is not cross-linked and still present in the starting preceramic polysiloxane.[25] As analyzed for AMK2 by in situ mass spectroscopy, in the same region methane is released shown by one of its mass fragments $m/z = 15$ in Fig. 2(c). Moreover, the masses $m/z = 29$, and $m/z = 43$ could be observed between 300 and 400 °C. Compared with databases these m/z values could be related to the main mass fragments of acetaldehyde, corresponding to a decomposition of the included solvent acetone. The expected mass fragments of water, methanol and ethanol could not be identified in this temperature region. The further weight loss, occurring between 550 and 900 °C features two relatively strong exothermic peaks which correspond to the polymer-to-ceramic conversion of the preceramic polymer and is due to the loss of methane followed by a loss of water and CO_2[25] as analyzed by in situ mass spectrometry revealing $m/z = 17/18$ for H_2O (Fig. 2(d)), $m/z = 12$ and $m/z = 44$ for CO_2 (Fig. 2(e)) which is formed in situ because of reactions between remaining organic functional groups and residual terminal hydroxyl groups of the composite. A pronounced broad exothermic DTA peak at about 1230 °C with an onset temperature of about 1090 °C together with a sharp exothermic peak at around 1310 °C as shown in Fig. 2(b) indicates the formation of δ- and θ-alumina and a subsequent crystallization of mullite, respectively.[21,26] Additionally, the X-ray spectra for this sample reveal that a significant crystallization process takes places between 1300 and 1400 °C (Fig. 3(b)).

X-ray powder diffraction patterns for the samples AMK1 and AMK2 are presented in Figs. 3 and 4. Accordingly, the observed reflexes of δ-alumina and γ-alumina are gaining in intensity with increasing pyrolysis temperature, from 1100 to 1300 °C. The difference between the two samples is related to the presence of two additional weak reflexes of mullite phase for AMK2 as depicted in Fig. 3. The samples annealed at 1400 and 1500 °C are crystalline with mullite as the major crystalline phase. A detailed Rietveld analysis for AMK1 showed that the ceramic matrix still contains a small amount of amorphous SiOC phase as also indicated by the amorphous halo around $2\Theta = 22°$, while for AMK2 the reflexes assigned to the mullite phase are identified exclusively. Rietveld refinement of the experimental diffraction pattern was used for the quantitative determination of all phases including mullite, amorphous silica-based phase and silicon carbide and the results of the refinements are highlighted in Table 1 and Fig. 5. The quantitative determination of the amorphous SiO_2-based component is done using the structure factor of cubic silica according to the literature.[27,28] As reported by Lutterotti et al.[28] silica glass may contain other elements that in principle can alter the Rietveld analysis. For our estimation of the amount of amorphous silica phase we neglected the presence of carbon and/or aluminium in SiO_2. The analysis of the X-ray diffraction pattern cannot resolve the crystalline phase of silicon carbide, however this phase is taken into account by the Rietveld

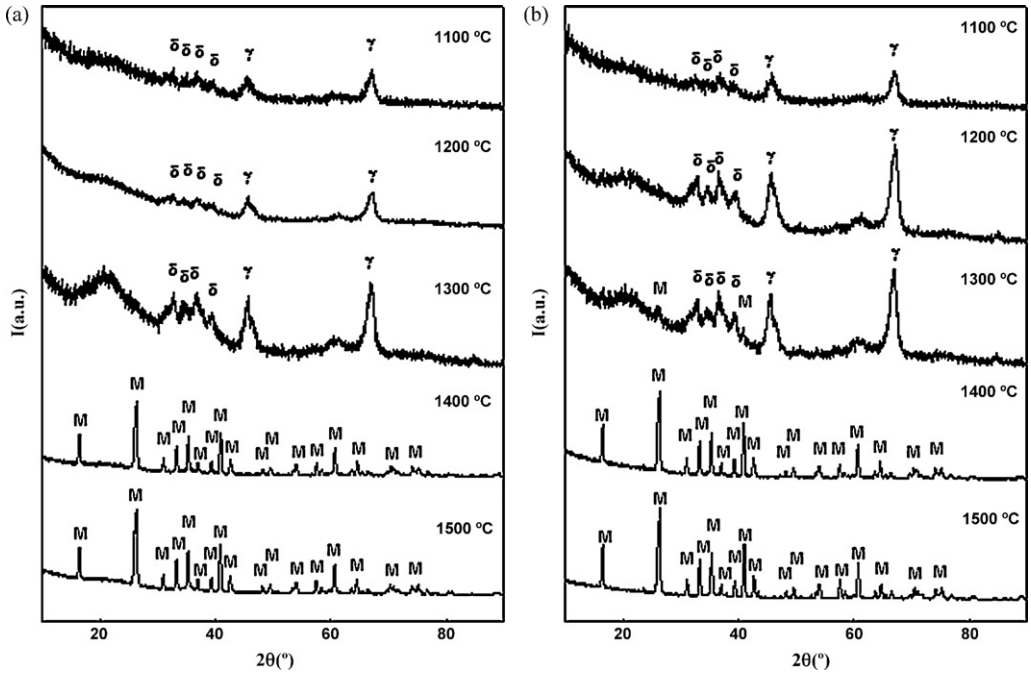

Fig. 3. X-ray diffraction analyses of the obtained ceramics for the samples: (a) AMK1 and (b) AMK2.

analysis as it has been found in the ceramic matrix with the help of micro-Raman analysis (see also Fig. 7).

The functionalized γ-alumina nanopowder used as filler in the AFMK1 and AFMK2 sample series evidently reduces the temperature of mullite formation, as can be seen from the X-ray spectra shown in Fig. 4. While the samples pyrolyzed at 1100 and 1200 °C reveal the same features as AMK1 and AMK2, the mullite phase segregates already after pyrolysis at 1300 °C. For AFMK2 approximately a 50% weight fraction of mullite is present in the matrix at this temperature (see Table 1). In addition a small reflex attributed to cristobalite is observed for this sample (1 wt% accordingly to Rietveld analysis). Besides mullite residual γ-alumina phase is also found for both samples at this temperature. Increasing the annealing temperature enhances the mullitization process which is completed between 1400 and 1500 °C (∼95 wt% of mullite and ∼5 wt% silicon carbide phase for the AFMK2/1500 °C composite). After annealing of the samples at 1400 and 1500 °C γ-alumina and cristobalite

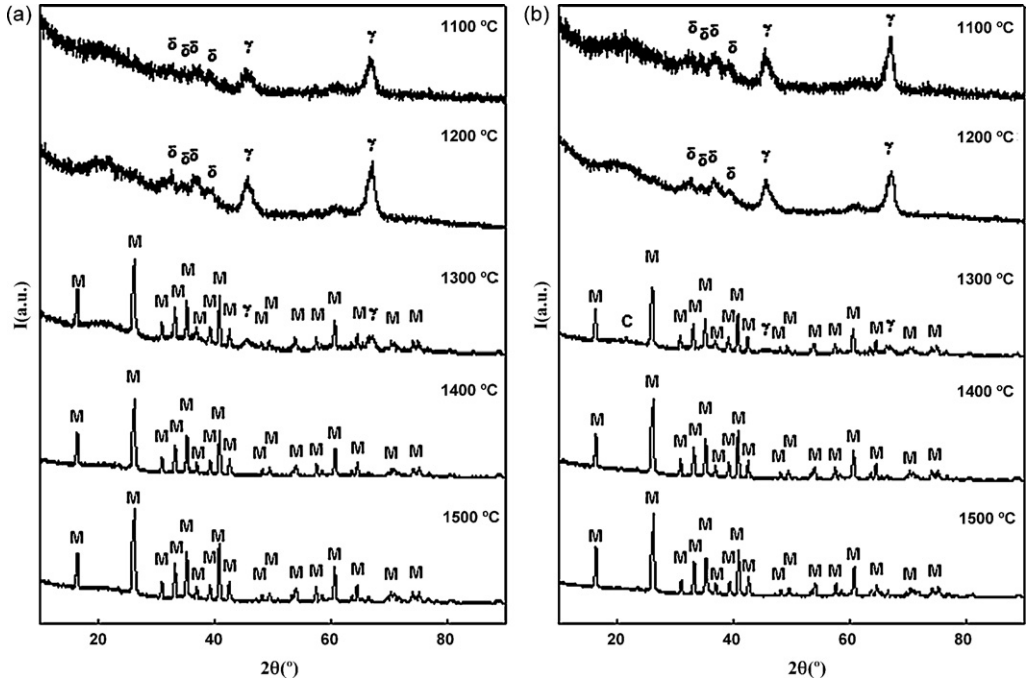

Fig. 4. X-ray diffraction analyses of the obtained ceramics for the samples: (a) AFMK1 and (b) AFMK2.

Table 1
Results of the quantitative phase analyses (wt%) derived from Rietveld refinement of the selected ceramic composite samples. Details of the Rietveld refinement are noted.

	Sample									
	AMK1		AMK2		AFMK1			AFMK2		
	1400 °C[a]	1500 °C[a]	1400 °C[a]	1500 °C[a]	1300 °C[a]	1400 °C[a]	1500 °C[a]	1300 °C[a]	1400 °C[a]	1500 °C[a]
Mullite	62.3	60.3	91.8	95.7	33.7	59.7	61.2	51.2	72.9	95.8
SiC	4.1	2.4	8.2	4.3	6.4	3.8	3.0	13.3	2.8	4.2
Amorphous SiO_2	33.6	37.3			53.1	36.4	35.8	29.0	24.3	
Cristobalite								1.0		
γ-Alumina					6.8			5.5		
R_p (%)	3.68	3.94	5.46	4.23	5.03	5.41	4.64	5.05	5.28	6.53
R_{wp} (%)	4.77	5.22	7.09	5.58	6.70	7.03	6.22	6.58	6.91	8.76
R_{wp} (expected) (%)	4.32	4.41	6.23	5.13	6.23	6.98	5.83	5.87	6.53	5.81
χ^2	1.22	1.40	1.29	1.18	1.16	1.01	1.14	1.26	1.12	2.28

[a] Annealing temperature.

are no longer found in the ceramic composites. The amorphous residue consisting of a SiOC phase detected for the two samples after pyrolysis at 1100 °C is diminished completely only for the AFMK2/1500 °C (Rietveld analysis, Table 1).

As depicted in Figs. 3 and 4 a high amount of alumina residue in the form of a mixture of γ- and θ-Al_2O_3 as well as an amorphous phase (silicate glass) was identified as the main remaining phases in the ceramic samples up to 1300 °C. That the γ-alumina phase could still be identified in the ceramic matrix annealed at 1300 °C is not surprising as it is known that amorphous SiO_2 can elevate the temperature of the γ-Al_2O_3-to-α-Al_2O_3 phase transformation.[29] The formation of α-Al_2O_3 (corundum) could not be detected in any of our sample mixtures. This finding suggests that a total conversion of the initial alumina phase into mullite was achieved. The fine dispersion of the γ-Al_2O_3 in the SiOC matrix additionally hinders the transition of the γ-phase into the stable α-phase.

The crystallite sizes of the mullite and of the silicon carbide phases estimated with the help of a Rietveld analysis and by the Scherrer equation are presented in Table 2. The crystallite size of the mullite phase remains almost unchanged during the heat treatment with values generally ranging from 60 to 90 nm and a singular value exceeding 160 nm for the AMK2 sample heat treated at 1500 °C. For the silicon carbide phase the crystallite size increases with rising temperature of the heat treatment but do not exceed a maximum value of 9 nm. Consequently, these results suggest the formation of a nanocomposite material. According to the information provided by the producer, the average particle size of the starting γ-alumina powder used in our experiments is around 13 nm, while the crystallite size of this powder calculated from the line broadening of the X-ray powder diffraction reflexes according to the Scherrer equation gives a value of 6–7 nm. The crystallite size calculated for the residual γ-alumina phase in the samples AFMK1 and AFMK2 pyrolyzed at 1300 °C is calculated to be 4 nm. The reduction of the γ-alumina crystallite size is assigned to the reaction of the SiOC matrix with the alumina particles to give mullite.

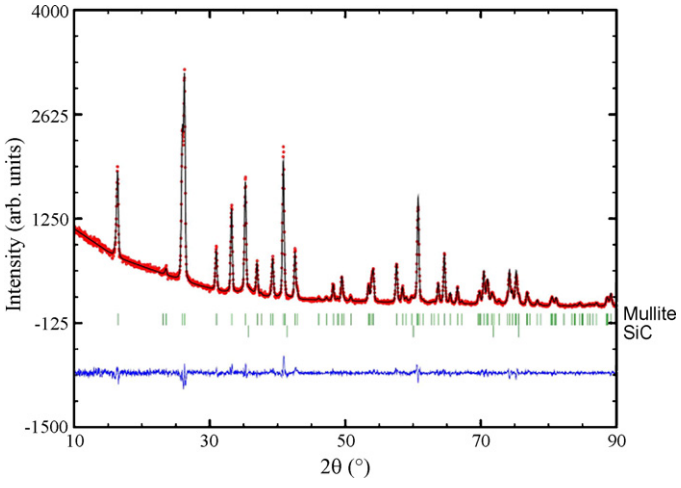

Fig. 5. Example of Rietveld pattern refinement for the sample AMK1 annealed at 1500 °C. Observed points are represented with circles, and the calculated pattern is shown with a full line. The difference pattern is shown at the bottom. Short vertical markers represent allowed reflexions. The Bragg reflexions for each phase are labelled on the right.

In order to quantify the elements present in the pyrolyzed mixture, elemental analyses data of the samples annealed at 1500 °C are listed in Table 3. It is found that the higher amount of used alumina filler reduces the total carbon content compared to that observed in SiOC ceramic.[25] According to the scheme reported by Harshe[30] the quantitative amount of alumina, silica, silicon carbide and carbon are derived from the elemental analysis data (Table 3). As analyzed by the amorphous halo in the XRD patterns of the samples AMK1 and AFMK1 the elemental analysis confirms that in the ceramic matrix a residual amount of 10–15 wt% of SiO_2 or SiOC phase is present, indicating that not enough Al_2O_3 filler was added to convert the entire silica into mullite. Thus, increasing the filler content achieves full transformation of silica into mullite (sample AMK2). Further fine tuning of the filler content can consequently result in the development of an alumina/silica free ceramic. In this context it is interesting to correlate the results obtained from the elemental analysis with the ones obtained with the help of the Rietveld analysis. In our case, a very good agreement between the two methods is reached for AMK2/1500 °C and AFMK2/1500 °C indicating that the mullite formation is completed. Therefore it can be concluded that the ceramic matrix of the two samples has to be

Table 2
Crystallite sizes (nm) calculated by Rietveld analyses for the selected ceramic samples. The crystallite size of γ-alumina in the samples AMK1 and AMK2 pyrolyzed at 1300 °C was calculated by the line broadening of the X-ray diffraction lines applying the Scherrer equation.

	Sample											
	AMK1			AMK2			AFMK1			AFMK2		
	1300 °C[a]	1400 °C[a]	1500 °C[a]	1300 °C[a]	1400 °C[a]	1500 °C[a]	1300 °C[a]	1400 °C[a]	1500 °C[a]	1300 °C[a]	1400 °C[a]	1500 °C[a]
Mullite		74	62		75	160	88	86	94	89	95	74
SiC		2.5	3.6		1	3.5	1.2	1.9	3.9	0.8	2.9	8.2
γ-Alumina	6			6			3.6			3.7		

[a] Annealing temperature.

Table 3
Elemental composition of the pyrolyzed products, empirical formula and theoretical weight percentage of the phases calculated for the ceramic samples.

Sample	Composition (wt%)				Empirical formula	Al_2O_3	SiO_2	Mullite	SiC	C_{free}
	Si	Al	O	C						
AMK1/1500 °C	21.09	29.40	44.13	5.38	$SiAl_{1.45}O_{3.67}C_{0.60}$	–	11.9	77.3	7.5	3.2
AMK2/1500 °C	15.90	36.22	45.73	2.15	$SiAl_{2.37}O_{5.05}C_{0.32}$	3.8	–	89.9	5.8	0.4
AFMK1/1500 °C	19.24	29.57	44.75	5.46	$SiAl_{1.60}O_{4.17}C_{0.66}$	–	14.6	77.7	3.2	4.5
AFMK2/1500 °C	16.05	34.30	45.99	3.66	$SiAl_{2.23}O_{5.03}C_{0.53}$	–	3.6	90.2	3.5	2.6

considered as a nanocomposite with a crystallite size of 160 and 75 nm for mullite as well as 4 and 8 nm for silicon carbide. In the case of the samples AMK1/1500 °C and AFMK1/1500 °C there is a discrepancy between the values obtained for the weight fractions of the crystalline phases, which is explained by the presence of a remaining amorphous SiOC phase in the ceramic nanocomposite matrix.

The micro-Raman spectra of all four pyrolyzed and annealed sample mixtures investigated here show nearly identical features. Therefore, the micro-Raman spectra for the AMK2 composite material are depicted in Fig. 6 for example. A first observation is that the intrinsic fluorescence of the samples pyrolyzed at 1100 and 1200 °C, hinders the acquisition of qualitatively appropriate spectra. The samples clearly exhibit two strong absorption bands located in the region of 1350 and 1582 cm^{-1}. In addition a band around 2700 cm^{-1} with lower intensity is analyzed in the samples obtained at 1300, 1400 and 1500 °C. These bands are characteristic for the so called G- and D-bands and illustrate the formation of graphitic-type carbon separated from the silicon oxycarbide (SiOC) matrix.[31] The G-band appears at 1582 cm^{-1} and is characteristic for graphite lattices. For poor crystalline graphite, additional bands are found: the disorder-induced D band (appears at 1350 cm^{-1} in the carbon aromatic structures with defects[32] and is sensitive to graphite intercalations[33]) and D′ band (appears at 1622 cm^{-1} as a shoulder peak of the G band and is also absent in highly crystalline graphite) as well as the second-order G′-band (located at 2700 cm^{-1} and is the second most intense feature in the Raman spectrum of completely ordered 3D graphite). Consequently, the most important information which can be deduced from the interpretation of the Raman spectra for all four samples is that some of the carbon in the ceramic matrix forms a sp^2-hybridized carbon network. This result indicates that the carbon network present in our samples should be found in a low crystalline state. After annealing of the samples at higher temperatures, carbon is found to be still enclosed in the ceramic matrix as it has been also concluded from the elemental analysis data.

While the X-ray powder diffraction measurements clearly evidenced the presence of mullite in all of the four ceramic

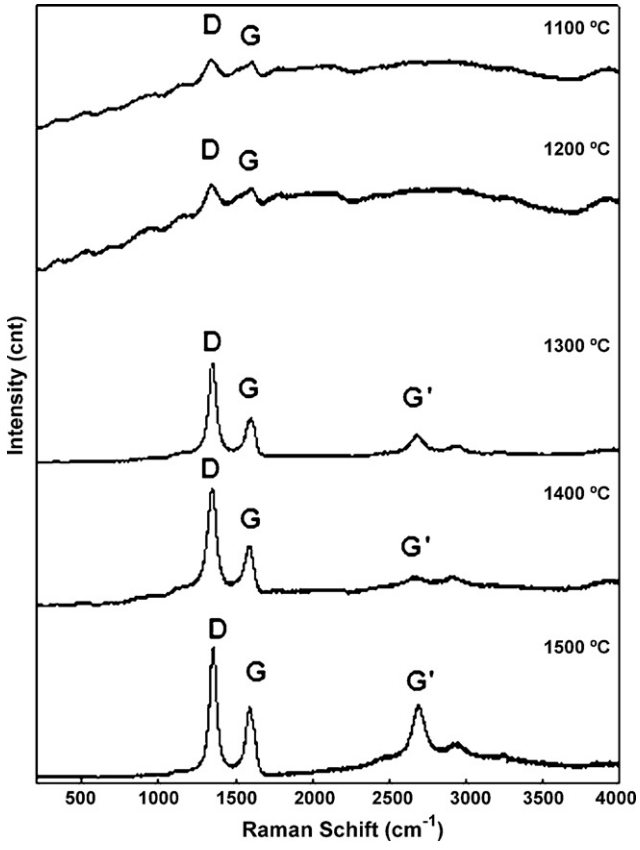

Fig. 6. Representative micro-Raman spectra of the selected sample AMK2 heat treated at different temperatures.

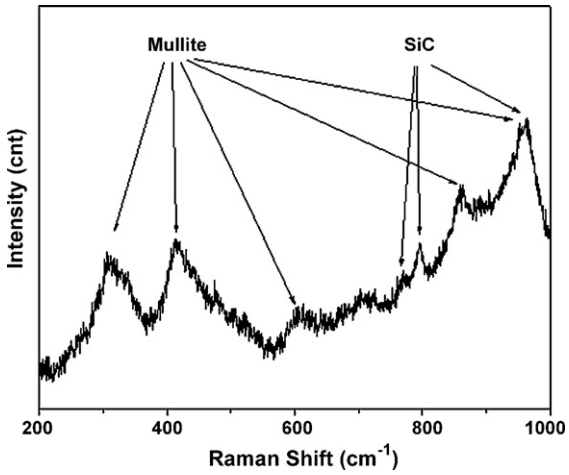

Fig. 7. Detail of the micro-Raman spectra of the selected sample AMK2 annealed at 1500 °C.

samples, the aluminosilicate $2SiO_2 \times 3Al_2O_3$ could not be evidenced by micro-Raman spectroscopy. Consequently a more detailed analysis was performed in the region 200–1000 cm^{-1} using a higher acquisition time (30 s) to obtain the Raman spectra of AMK2/1500 °C (Fig. 7). This approach proved to be successful and mullite could be identified. Five characteristic Raman peaks with broad line shapes were analyzed which are in accordance with the typical bands related to mullite (see Fig. 7).[34,35] Moreover, silicon carbide could be assigned by the characteristic broad peaks around 796 and 970 cm^{-1}. The lines correspond to the transversal optical TO and longitudinal optical LO modes indicating the presence of the cubic β-SiC polymorph (3C–SiC). A weak satellite Raman peak at around 765 cm^{-1} is assigned also to α-SiC polytypes.[36] In the region of 970 cm^{-1}, the silicon carbide peak is overlapping with that of the characteristic peaks of the mullite phase. The Raman scattering efficiency of graphite in comparison with that of silicon carbide is 20 times higher, therefore the silicon carbide Raman fingerprint is difficult to be observed.

The typical microstructures of the bulk samples warm pressed, pyrolyzed at 1300 °C in Ar and finally annealed at 1500 °C under Ar as investigated by SEM for the samples AMK2 and AFMK2 are shown in Fig. 8. It is evident that the samples are characterized by some residual porosity. Preliminary results regarding the fracture toughness derived from the Vickers indentations (see Fig. 8) of the ceramic samples AMK2 and AFMK2 yielded experimental values of $K_{IC} = 3.3\ MPa\ m^{1/2}$ and $K_{IC} = 2.6\ MPa\ m^{1/2}$, respectively. More detailed results related to the mechanical studies will be published in a separate paper. The images taken with high magnification in the pore areas show the presence of round shaped particles with sizes below 100 nm.

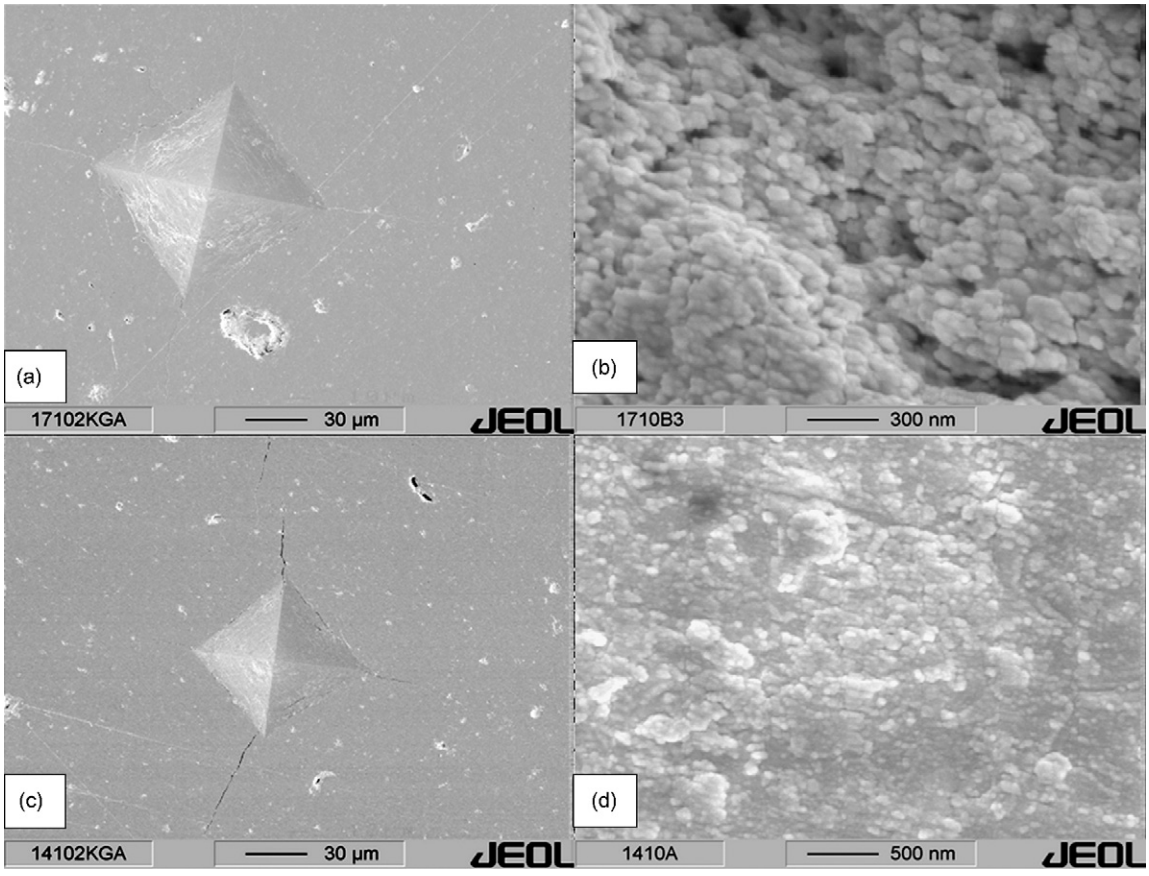

Fig. 8. Scanning electron microscopic micrographs of the samples AMK2 ((a) 400× and (b) 50,000× magnification) and AFMK2 ((c) 430× and (d) 30,000× magnification) after heat treatment at 1500 °C. The surface morphology of polished sample surfaces, cases (a) and (c) show also a Vickers indentation which was performed with a load of 2 kg. The higher magnifications (b) and (d) show the interior of the pores of the bulk specimens.

The microstructure of the samples AMK2 and AFMK2 annealed at 1500 °C was also investigated by means of TEM coupled with high-resolution imaging (HRTEM) (Fig. 9). In the TEM studies the presence of mullite matrix grains was confirmed by selected-area diffraction (SAD). The bright-field image (Fig. 9(a)) (Apertur $(2\,\mathrm{nm})^{-1}$) shows an overview of the microstructure and Fig. 9(b) represents a dark field image of another area with one randomly selected diffraction reflex. It

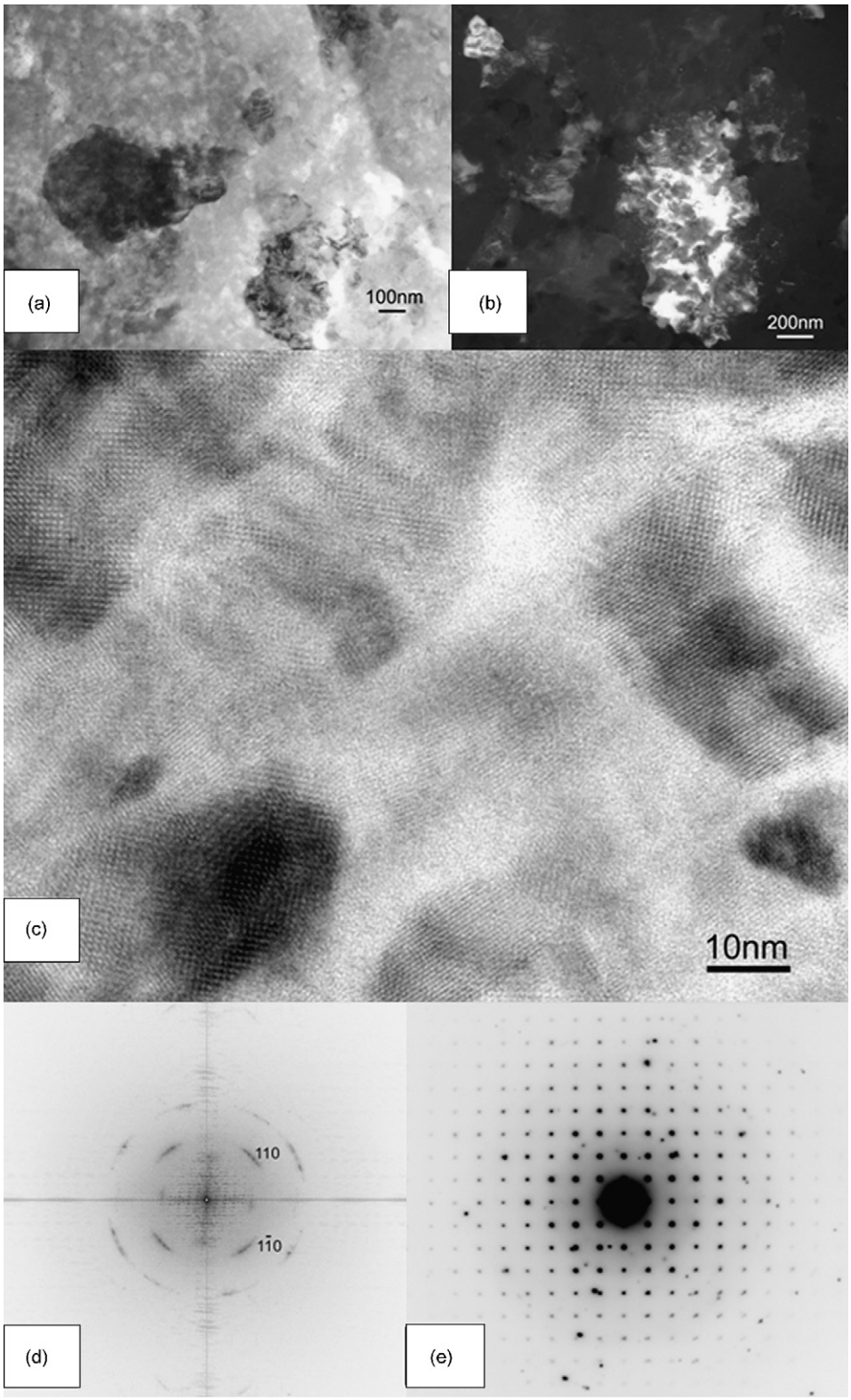

Fig. 9. Bright field (a) and dark field (b) TEM micrographs of the ceramic sample AFMK2 annealed at 1500 °C. High-resolution TEM image of the mullite matrix (c). Diffraction pattern obtained by Fourier-transformation of the polycrystalline area shown in c (d). Electron diffraction image of a larger single crystal confirming the presence of mullite (e).

is evident that the brightness and therewith the orientation of the single crystals are strongly fluctuating. The analysis of the high resolved TEM images (Fig. 9(c)) displays that the orientation of the single crystals can be fanned out with as far as 20° and typically with a size up to 50 nm. Fig. 9(d) shows the Fourier-transformation of an area of about 200 nm in diameter as depicted in Fig. 9(c). The electron diffraction image of a larger particle given in Fig. 9(e) proofs that single crystals in the size of 200 nm in diameter are also present.

The crystallite size of the SiC as deduced from the X-ray diffractograms is estimated to be smaller than 10 nm. Because of the small crystallite size together with its (i) low concentration, (ii) strong textured contrast in the mullite matrix and (iii) similar absorption for the related constituting elements it was not possible to localize the SiC phase in our TEM studies. This result also indicates the presence of a homogeneous distribution of the SiC nano-particles. Moreover, no amorphous material was detected in the TEM investigations which is consistent with the reported XRD data and suggests that the formation of mullite was completed after annealing at 1500 °C for 3 h.

The amount of the open porosity of the ceramics is summarized in Table 4 together with the respective densities as determined in form of the bulk density and according to the Archimedes method using water as infiltrating medium. The open porosity decreases with increasing pyrolysis temperature and the skeletal density increases with temperature. The ceramic samples of the mixture AMK2 exhibit the highest open porosity (~20%), while the other samples show a relatively low open porosity (between 2 and 8%). The theoretical density of the two crystalline samples AMK2/1500 °C and AFMK2/1500 °C based on the elemental analysis data and on the calculated phase fractions (Table 3) is estimated to be of 3.09 g/cm^3 and 3.04 g/cm^3, respectively. Therefore, in two cases the skeletal density measured by the Archimedes method amounts 97 and 92% of the theoretical density, respectively. Taking into account the measured porosity data and the microstructural studies obtained by the SEM and TEM investigations shown in Figs. 8–10, we can conclude that the synthesized mullite/SiC nanocomposites can be well densified and contain a limited amount of pores.

Table 4
Density and porosity values for the prepared samples. The amount of open porosity was determined from the bulk density and from the density measured after the Archimedes method.

Sample	ρ_{bulk} (g/cm^3)	ρ_{arch} (g/cm^3)	Open porosity (%)
AMK1			
1300 °C	2.37	2.52	6
1400 °C	2.51	2.59	3
1500 °C	2.64	2.70	2
AMK2			
1300 °C	2.17	2.90	25
1400 °C	2.27	2.92	22
1500 °C	2.34	2.97	21
AFMK1			
1300 °C	2.43	2.54	4
1400 °C	2.55	2.63	3
1500 °C	2.55	2.63	3
AFMK2			
1300 °C	2.48	2.7	8
1400 °C	2.51	2.7	7
1500 °C	2.65	2.82	6

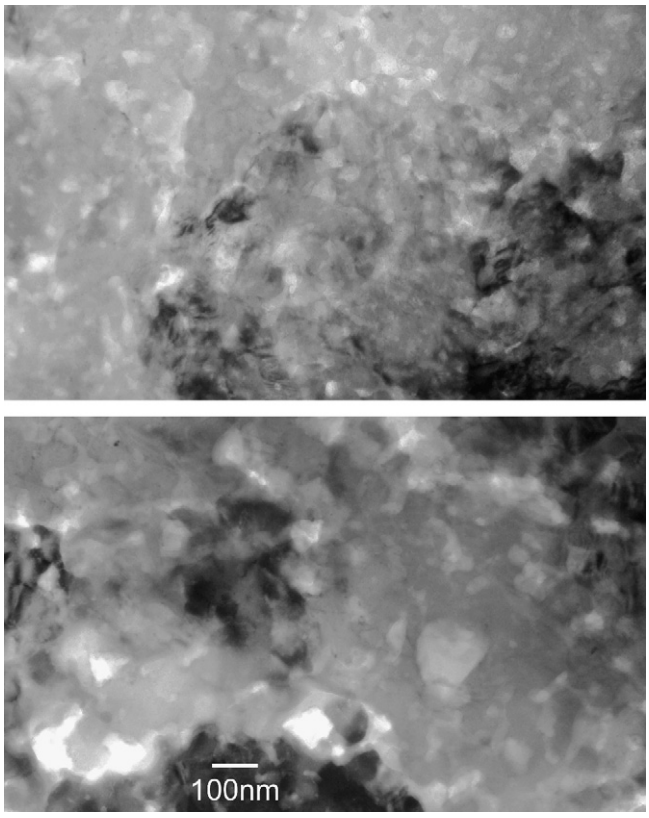

Fig. 10. TEM micrographs of the ceramic sample AFMK2 annealed at 1500 °C (up) and of AMK2 annealed at 1500 °C.

In all the TEM images it is obvious that, independent from the orientation of the scattering absorption contrast, the material is interpenetrated with pores. It seems that these voids have the characteristics of closed pores rather that of open channels. For the sample AFMK2 the pores are smaller but more numerous than in the case of the sample AMK2 (Fig. 10).

The microstructural development of the ceramic nanocomposite is subject to the composition of the starting compound. An aspect of more general interest in this context is the chance to carry out systematic studies on the interaction between the alumina filler and the preceramic polymer. According to our results, the rate of mullite formation and the ceramic microstructure is significantly influenced by the type of nano-filler particles. In particular, the use of nano-γ-Al_2O_3 filler functionalized with octylsilane provides a higher amount of crystalline mullite phase at lower temperatures as in the case of non-functionalized γ-Al_2O_3 filler. The hydrophobic contact surface of the filler particles seems to increase the reactivity of alumina with respect to the preceramic polymer during pyrolysis. Additionally the homogeneity of the starting mixtures is enhanced for the functionalized alumina filler, which results in a lower crystallite size of the mullite phase in the obtained ceramic as found in the case of the samples AMK2/1500 °C (160 nm) and AFMK2/1500 °C

(75 nm). The preceramic polysiloxane provides the raw material necessary for the formation of mullite/silicon carbide nanocomposites. The future task in this context is to study cooperative phenomena between the polymer and ceramic filler particles in order to understand the interaction of the functionalized groups attached to the alumina surface with the preceramic polymer during the ceramization process.

4. Conclusions

A new strategy has been followed to synthesize mullite–SiC-based nanocomposite ceramics using alumina or functionalized alumina nano-sized particles as filler together with a commercially available polymer. Mullite formation was achieved at unusual low temperatures due to the high reactivity of the nano-alumina filler particles towards the silica rich ceramic matrix formed from the polysiloxane fraction. This novel process enables the formation of dense mullite–SiC nanocomposites with relatively low porosity using polymer forming techniques. The microstructural results indicate that SiC as well as the segregated carbon hinders the growth of the mullite crystals. In our mullite/SiC nanocomposite the crystallite size of mullite was analyzed to be between 50 and 200 nm while in pure polysiloxane-derived mullite obtained by pyrolysis in air the particle size was determined to be in the micrometer range (ca. 1 μm).[23] The achieved results are in particular of interest for the production of complex shaped high temperature and corrosion resistant ceramic devices as well as for advanced fibers and fiber-reinforced composites, microelectronic substrates and other applications.

Acknowledgments

The work reported here is part of the Priority Program "Nanoscaled Inorganic Materials by Molecular Design: New Materials for Advanced Technologies" (DFG-SPP 1181) funded by the Deutsche Forschungsgemeinschaft, Bonn, Germany. R.R. also thanks the Fonds der Chemischen Industrie, Frankfurt, Germany, for financial support.

References

1. Sternitzke, M., Review: structural ceramic nanocomposites. *J. Eur. Ceram. Soc.*, 1997, **17**, 1061–1082.
2. Schneider, H., Schreuer, J. and Hildmann, B., Structure and properties of mullite—a review. *J. Eur. Ceram. Soc.*, 2008, **28**, 329–344.
3. Aksay, I. A., Dabbs, D. M. and Sarikaya, M., Mullite for structural, electronic, and optical applications. *J. Am. Ceram. Soc.*, 1991, **74**, 2343–2356.
4. Niihara, K., New design concept of structural ceramics–ceramic nanocomposites. *J. Ceram. Soc. Jpn.*, 1991, **99**, 974–982.
5. Gao, L., Jin, X., Kawaoka, H., Sekino, T. and Niihara, K., Microstructure and mechanical properties of SiC–mullite nanocomposite prepared by spark plasma sintering. *Mater. Sci. Eng.*, 2002, **A334**, 262–266.
6. Ando, K., Furusawa, K., Chu, M. C., Hanagata, T., Tuji, K. and Sato, S., Crack-healing behaviour under stress of mullite/silicon carbide ceramics and the resultant fatigue strength. *J. Am. Ceram. Soc.*, 2001, **84**, 2073–2078.
7. Takahashi, K., Uchiide, K., Kimura, Y., Nakao, W., Ando, K. and Yokouchi, M., Threshold stress for crack healing of mullite reinforced by SiC whiskers and SiC particles and resultant fatigue strength at the healing temperature. *J. Am. Ceram. Soc.*, 2007, **90**, 2159–2164.
8. Ando, K., Chua, M.-C., Tsuji, K., Hirasawa, T., Kobayashi, Y. and Sato, S., Crack healing behaviour and high-temperature strength of mullite/SiC composite ceramics. *J. Eur. Ceram. Soc.*, 2002, **22**, 1313–1319.
9. Soraru, G. D., Kleebe, H.-J., Ceccato, R. and Pederiva, L., Development of mullite–SiC nanocomposites by pyrolysis of filled polymethylsiloxane gels. *J. Eur. Ceram. Soc.*, 2000, **20**, 2509–2517.
10. Renlund, G. M., Prochazka, S. and Doremus, R. H., Silicon oxycarbide glasses. Part I. preparation and chemistry. *J. Mater. Res.*, 1991, **6**, 2716–2722.
11. Renlund, G. M., Prochazka, S. and Doremus, R. H., Silicon oxycarbide glasses. Part II. Structure and properties. *J. Mater. Res.*, 1991, **6**, 2723–2734.
12. Greil, P., Active-filler-controlled pyrolysis of preceramic polymers. *J. Am. Ceram. Soc.*, 1995, **78**, 835–848.
13. Greil, P., Polymer derived engineering ceramics. *Adv. Eng. Mater.*, 2000, **2**, 339–348.
14. Riedel, R., Passing, G., Schönfelder, H. and Brook, R. J., Synthesis of dense silicon-based ceramics at low temperatures. *Nature*, 1992, **355**, 714–717.
15. http://www.ill.eu/sites/fullprof/index.html.
16. Balzar, D. and Ledbetter, H., Crystal structure and compressibility of 3–2 mullite. *Am. Mineral.*, 1993, **78**, 1192–1196.
17. Kawamura, T., Silicon carbide crystals grown in nitrogen atmosphere. *Miner. J. (Jpn.)*, 1965, **4**, 333–355.
18. Peacor, D. R., High-temperature single-crystal study of the cristobalite inversion. *Phase Transitions*, 1992, **38**, 127–220.
19. Zhou, R.-S. and Snyder, R. L., Structures and transformation mechanisms of the eta, gamma and theta transition aluminas. *Acta Cryst. B*, 1991, **47**, 617–630.
20. Griggio, F., Bernardo, Colombo, E. P. and Messing, G. L., Kinetic studies of mullite synthesis from alumina nanoparticles and a preceramic polymer. *J. Am. Ceram. Soc.*, 2008, **91**, 2529–2533.
21. Bernardo, E., Colombo, P., Pippel, E. and Woltersdorf, J., Novel mullite synthesis based on alumina nanoparticles and a preceramic polymer. *J. Am. Ceram. Soc.*, 2006, **89**, 1577–1583.
22. Bartsch, M., Saruhan, B., Schmücker, M. and Schneider, H., Novel low-temperature processing route of dense mullite ceramics by reaction sintering of amorphous SiO_2-coated γ-Al_2O_3 particle nanocomposites. *J. Am. Ceram. Soc.*, 1999, **82**, 1388–1392.
23. Michalet, T., Parlier, M., Beclin, F., Duclos, R. and Crampon, J., Elaboration of low shrinkage mullite by active filler controlled pyrolysis of siloxanes. *J. Eur. Ceram. Soc.*, 2002, **22**, 143–152.
24. Suttor, D., Kleebe, H.-J. and Ziegler, G., Formation of mullite from filled siloxanes. *J. Am. Ceram. Soc.*, 1997, **80**, 2541–2548.
25. Harshe, R., Balan, C. and Riedel, R., Amorphous Si(Al)OC ceramic from polysiloxanes: bulk ceramic processing, crystallization behaviour and applications. *J. Eur. Ceram. Soc.*, 2004, **24**, 3471–3482.
26. Ivankovic, H., Tkalcec, E., Nass, R. and Schmidt, H., Correlation of the precursor type with densification behavior and microstructure of sintered mullite ceramics. *J. Eur. Ceram. Soc.*, 2003, **23**, 283–292.
27. Le Bail, A., Modelling the silica glass structure by the Rietveld method. *J. Non-Cryst. Solid*, 1995, **183**, 39–42.
28. Lutterotti, L., Ceccato, R., Dal Maschio, R. and Pagani, E., Quantitative analysis of silicate glass in ceramic materials by the Rietveld method. *Mater. Sci. Forum*, 1998, **278–281**, 87–92.
29. Saito, Y., Takei, T., Hayashi, S., Yasumori, A. and Okada, K., Effects of amorphous and crystalline SiO_2 additives on γ-Al_2O_3-to-α-Al_2O_3 phase transitions. *J. Am. Ceram. Soc.*, 1998, **81**, 2197–2200.
30. Harshe, R., Synthesis and processing of amorphous Si(Al)OC bulk ceramics: high temperature properties and applications. PhD thesis. Technische Universität Darmstadt, Darmstadt, Germany, 2004.
31. Pimenta, M. A., Dresselhaus, G., Dresselhaus, M. S., Cancado, L. G., Jorio, A. and Saito, R., Studying disorder in graphite-based systems by Raman spectroscopy. *Phys. Chem. Chem. Phys.*, 2007, **9**, 1276–1291.
32. Beny-Bassez, C. and Rouzaud, J. N., Characterization of carbonaceous materials by correlated electron and optical microscopy and Raman microspectroscopy. *Scan. Electron Microsc.*, 1985, **1**, 119–132.

33. Dresselhaus, M. S. and Dresselhaus, G., Light scattering in graphite intercalation compounds. In *Light scattering in solids III*, ed. M. Cardona and G. Guntherodt. *Topics in Applied Physics*, *vol. 51*. Springer-Verlag, Berlin, 1982, pp. 3–57.
34. Shoval, S., Boudeulle, M., Yariv, S., Lapides, I. and Panczer, G., Micro-Raman and FT-IR spectroscopy study of the thermal transformations of St. Claire dickite. *Opt. Mater.*, 2001, **16**, 319–327.
35. Rüscher, C. H., Phonon spectra of 2:1 mullite in infrared and Raman experiments. *Phys. Chem. Miner.*, 1996, **23**, 50–55.
36. Gouadec, G. and Colomban, P., Non-destructive mechanical characterization of SiC fibers by Raman spectroscopy. *J. Eur. Ceram. Soc.*, 2001, **21**, 1249–1259.